Journal of Molecular Liquids 368 (2022) 120612

Contents lists available at ScienceDirect

Journal of Molecular Liquids

journal homepage: www.elsevier.com/locate/molliq

Kinetics of cold crystallization in two liquid crystalline fluorinated homologues exhibiting the vitrified smectic C_A^* phase

Aleksandra Deptuch [a,*], Małgorzata Jasiurkowska-Delaporte [a], Magdalena Urbańska [b], Stanisław Baran [c]

[a] Institute of Nuclear Physics Polish Academy of Sciences, PL-31342 Kraków, Poland
[b] Institute of Chemistry, Military University of Technology, PL-00908 Warsaw, Poland
[c] M. Smoluchowski Institute of Physics, Jagiellonian University, PL-30348 Kraków, Poland

ARTICLE INFO

Article history:
Received 4 April 2022
Revised 3 October 2022
Accepted 13 October 2022
Available online 19 October 2022

ABSTRACT

Dielectric relaxation processes in the supercooled antiferroelectric smectic C_A^* phase and crystallization kinetics of two chiral fluorinated 5HF6 and 6HF6 compounds from the same homologous series are investigated. Fragility parameters are determined from the relaxation time of the α-process, including τ_{HN} from the Havriliak-Negami formula and τ_{peak} denoting the position of the absorption peak. The coupling coefficient ξ between the characteristic time of isothermal cold crystallization and relaxation time of the α-process is obtained. Despite similar values of the fragility index, the even 6HF6 homologue undergoes cold crystallization much faster than the odd 5HF6 homologue, with significantly different ξ coefficients. Influence of the relaxation time of the P_H process (anti-phase phason) in the smectic C_A^* phase on the crystallization kinetics is presumed.

1. Introduction

Compounds which have in their phase sequence the smectic C_A^* (SmC_A^*) phase with a high tilt angle of 42-45°, named the orthoconic antiferroelectric liquid crystals (OAFLCs), are suitable for LC displays because of their optical uniaxiality leading to a good quality of the dark state [1–3]. In order to find the optimal components of the OAFLC mixtures, systematic studies of the chiral smectogenic compounds have been performed over years to find correlations between their molecular structure and properties [4–10]. The best choice are these compounds which exhibit the SmC_A^* phase in a broad temperature range and which do not crystallize in the room temperature.

This study includes two homologues, 5HF6 and 6HF6, from the mHF6 series of fluorinated chiral liquid crystalline compounds [5,6,10] (abbreviated also as 3FmHPhF or 3FmHPhF6), see Fig. 1. The mHF6 compounds were used to prepare several orthoconic liquid crystalline mixtures [6,11]. It has been also shown [10,12] that mHF6 homologues with m = 5, 6, 7 exhibit the vitrified SmC_A^* phase even for slow cooling. The kinetics of the cold crystallization of 7HF6 was studied in details [13] and the dielectric spectroscopy results for this compound enabled determination of the fragility index $m_f \approx 100$ [12]. For 5HF6 and 6HF6, the dielectric spectra collected down to 219 K did not permit determination of m_f with a reasonable certainty. The aim of this paper is the study of the dielectric relaxation processes in mHF6 (m = 5, 6) in low temperatures, down to 173 K, including the α-process in the SmC_A^* phase and the β-process in the SmC_A^* glass. We are going also to present results regarding the crystallization kinetics of 5HF6 and 6HF6, and discuss the influence of the $-C_mH_{2m}-$ chain length on the glassforming properties of these compounds.

Broadband dielectric spectroscopy (BDS), the main experimental method of this study, is used frequently in investigations of the glass transition. From the BDS spectra one can determine the temperature dependence of the relaxation times of various molecular and collective processes in a studied material [14–18]. For the liquid crystals with para-, ferro- and antiferroelectric properties, the BDS method is helpful in identification of particular phases [19–21]. Relaxation processes can be described by the Havriliak-Negami formula in the frequency domain [22] or by the Kohlrausch-Williams-Watts function in the time domain [23]. The relaxation process characteristic of glassformers is the α-process [14–18]. The dielectric absorption peak of the α-process plotted as a function of $\ln f$ has in most of cases an asymmetric shape, wider at the high-frequency side. The temperature dependence of its relaxation time τ_α is usually non-Arrhenius and it is described by the Vogel-Fulcher-Tammann formula $\tau_\alpha(T) = \tau_0 \exp(B/(T - T_V))$ [14–18]. Based on the $\tau_\alpha(T)$ dependence, one can determine the fragility index m_f of the glassformer:

* Corresponding author.
E-mail address: aleksandra.deptuch@ifj.edu.pl (A. Deptuch).

https://doi.org/10.1016/j.molliq.2022.120612
0167-7322/

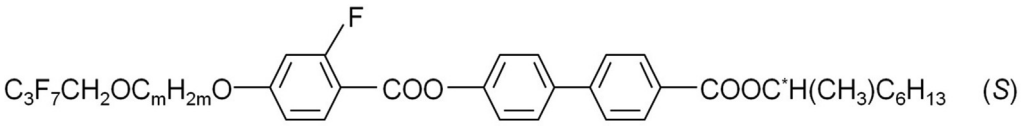

Fig. 1. Molecular formula of the mHF6 compounds (m = 5, 6 in this study).

$$m_f = \left.\frac{d\log_{10}\tau_\alpha(T)}{d(T_g/T)}\right|_{T_g} = \frac{BT_g}{(T_g - T_V)^2 \ln 10} \quad (1)$$

where the glass transition temperature T_g is defined as $\tau_\alpha(T_g)$ = 100 s [24]. Glasses with low m_f (strong glasses) are expected to have a smaller tendency to crystallization than fragile glasses with large m_f [25]. Experimental fragilities of the liquid crystalline glassformers cover a wide range [12,26–34], from m_f = 16 (Arrhenius behavior of τ_α) [26] to large fragilities up to 150 [30,31,33].

On the high-frequency side of the α-process, there is in some materials the secondary β-process. The dielectric absorption peak related to the β-process is very wide and usually symmetric in the ln$f$ domain. The relaxation time τ_β has the Arrhenius dependence on temperature [15–18]. The β-process can arise from the movements of the whole molecules (genuine Johari-Goldstein process) or from intra-molecular rotations (pseudo-JG process) [35,36]. If the β-process is a genuine JG process, then the pre-exponential factor τ_0 in the Arrhenius dependence of τ_β and its activation energy E_β, as well as the n' parameter of the KWW function describing the α-process, are expected to fulfill the equation [37]:

$$\frac{E_\beta}{RT_g} = 2.303(2 - 13.7n' - \log_{10}\tau_0) \quad (2)$$

In this paper, the BDS method is used to investigate the relaxation processes in the supercooled SmC_A^* phase and during the cold crystallization of 5HF6 and 6HF6 in non-isothermal and isothermal conditions. The characteristic time of isothermal cold crystallization, determined using the Avrami model [38–40], is compared with the relaxation time of the α-process to obtain the coupling coefficient between them [41,42]. The BDS results are completed with the X-ray diffraction (XRD) results which facilitate the observation of transitions between the crystal phases after non-isothermal cold crystallization.

2. Experimental details

The synthesis route of the mHF6 compounds is described in other publications [5,6].

XRD patterns in the 2θ = 2-30° range were collected for the samples in capillaries (borosilicate glass, diameter of 0.3 mm) with Empyrean 2 (PANalytical) diffractometer using CuKα radiation and Debye-Scherrer geometry. Temperature was controlled by Cryostream 700 Plus (Oxford Cryosystems) attachment. The samples were heated to the isotropic liquid and cooled down to 173 K at 6 K/min, then the measurements were done on heating. The collection of one diffraction pattern lasted ca. 14 min, including temperature stabilization, and the rate of temperature change between measurements was 6 K/min. Data analysis was done in WinPLOTR program [43]. The systematic error in 2θ was corrected on the basis of the positions of the 1st, 2nd and 3rd order peaks from the smectic layers at 173 K.

XRD pattern of the 6HF6 sample after melt crystallization at the room temperature was collected for the flat sample with X'Pert PRO diffractometer using CuKα radiation and Bragg-Brentano geometry.

BDS measurements in the 0.1–10^7 Hz range were carried out on Novocontrol Technologies spectrometer. The samples of ca. 70 μm thickness were contained between gold electrodes. Dielectric spectra were registered on heating to 333 K after fast cooling from the isotropic liquid phase to 173 K. Afterwards, the isothermal cold crystallization kinetics was investigated by cooling the melted samples down to 173 K, heating up to a selected crystallization temperature T_{cr} (251, 253, 255 or 257 K) and collection of the BDS spectra in this temperature during crystallization. In all measurements, the collection of a single BDS spectrum lasted ca. 6 min, including the temperature stabilization, and the rate of temperature change between measurements was set to 5 K/min.

3. Results and discussion

3.1. Non-isothermal cold crystallization

3.1.1. XRD patterns

Diffraction patterns of 5HF6 and 6HF6 (Fig. 2) were collected on heating after cooling the sample from 393 K (isotropic liquid) to 173 K (SmC_A^* glass). The characteristic distances d determined from the low-angle diffraction peaks are presented in Fig. 3 (see Fig. S1 in Supplementary Material for details). For both compounds, a low-angle peak at 2θ = 2.8–3.0° is related to the smectic layer order [44]. This peak is visible between 173 K and the cold crystallization temperature, and also above the melting temperature of a crystal. The glass softening at $T_g \approx 230$ K is very weakly visible in the dependence of the integrated intensity of the peak at 2θ = 2.8–3.0° on temperature (Fig. 3). The beginning of the cold crystallization of 5HF6 is observed at 253 K as arising of a sharp diffraction peak at 2θ = 17.2° (Fig. 2a). At 278 K, the Cr3 phase melts and another crystal phase appears, denoted as Cr2, which is indicated e.g. by arising of a peak at $2\theta \approx 4.1°$ (Fig. 2a, the triangles in Fig. 3a). The peak at 2θ = 2.9–3.0° increases in intensity during the development of the Cr3 and Cr2 phases. The d value slightly decreases in the temperature range of the Cr2 phase and increases to the previous value in the Cr2 phase (the circles in Fig. 3a). It indicates that the characteristic distance in the crystal structures of Cr3 and Cr2 is similar to the smectic layer spacing. In the XRD patterns collected at 293 K and 298 K, another low-angle peak at 2θ = 2.8–2.9° appears, which is a sign of another crystal phase, Cr1, which coexists with Cr2 until melting (the rhombs in Fig. 3a). In the whole temperature range of 253–298 K, where the crystal phases of 5HF6 are observed, there is a wide diffuse maximum at $2\theta \approx 19°$ related to a short-range order in the smectic layers [44]. It means that the crystallization of 5HF6 is not completed and some fraction of the sample stays in the SmC_A^* phase. For 6HF6, the signs of cold crystallization are also observed at 253 K. The characteristic peak of the Cr3 phase is located as 2θ = 5.7° (Fig. 2b). The low-angle peak at 2θ = 2.8–2.9° increases in intensity in the temperature range of the Cr3 phase (the circles in Fig. 2b), indicating that the characteristic distance in the crystal structure of Cr3 is the same as the smectic layer spacing. Another crystal phase, Cr2, has the characteristic peak at 2θ = 3.0°, observed in the 268–278 K range (the rhombs in Fig. 3b). Finally, the Cr1 phase, with the characteristic peak at 2θ = 4.2°, develops at 278 K and the sample stays in the Cr1 phase until melting.

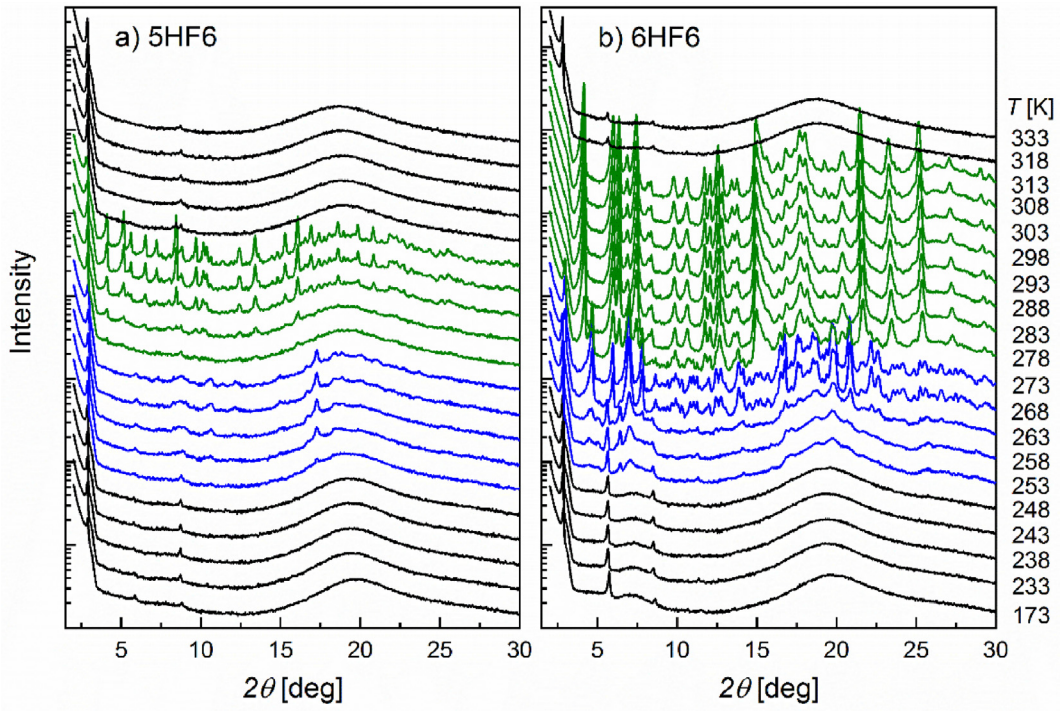

Fig. 2. Selected diffraction patterns of 5HF6 (a) and 6HF6 (b) collected on heating in the 173–333 K range. The temperature scale on right applies to both compounds. Intensities are in the logarithmic scale.

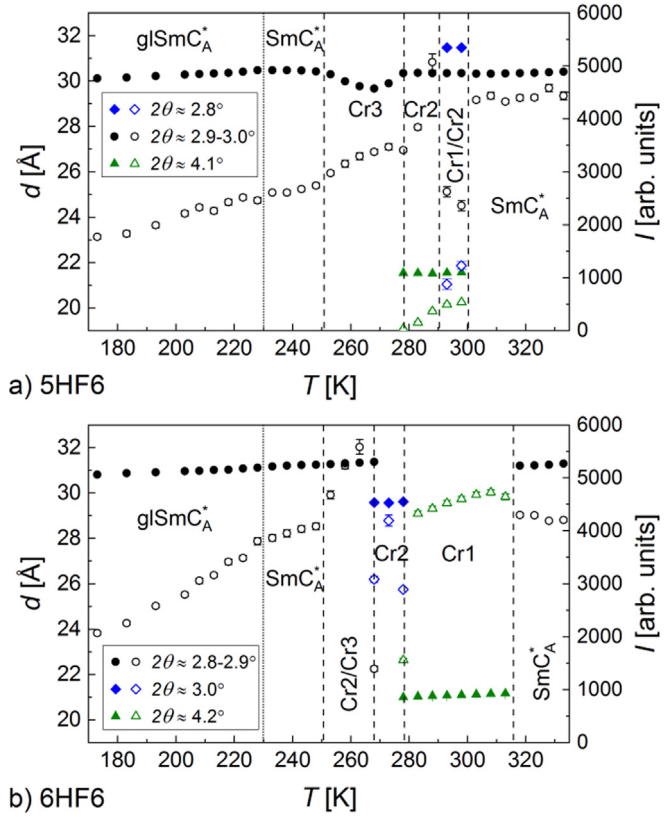

Fig. 3. Characteristic distances d (solid symbols) and integrated intensities I (open symbols) determined from the low-angle peaks in the XRD patterns of 5HF6 (a) and 6HF6 (b). The glass transition temperature $T_g \approx 230$ K was determined from the BDS results.

3.1.2. BDS spectra

Analysis of the BDS spectra of 5HF6 and 6HF6 (Fig. 4) was done by fitting the Cole-Cole [45] or Havriliak-Negami [22] formulas:

$$\varepsilon^*(f) = \varepsilon_\infty + \sum_j \frac{\Delta\varepsilon_j}{\left(1 + (2\pi i f \tau_{HNj})^{1-a_j}\right)^{b_j}} - \frac{iS}{(2\pi f)^{n_1}} \quad (3)$$

where the shape parameters a_j, b_j between 0 and 1, dielectric strength $\Delta\varepsilon_j$ and relaxation time τ_{HNj} describe each relaxation process, ε_∞ is the dielectric dispersion in a high-frequency limit and the S, n_1 parameters describe the conductivity contribution at low frequencies. While fitting the cr-I process in a crystal phase of 6HF6 in the 283–309 K range, the contribution from the electrodes' capacity $C/(2\pi f)^{n_2}$, where C and n_2 are fitting parameters, had to be included as well [14]. For $b = 1$ (Cole-Cole formula), the distribution of τ_{HN} is symmetric in the $\ln f$ domain and its width increases with increasing a. For $b < 1$ (Havriliak-Negami formula), the distribution of τ_{HN} is asymmetric in the $\ln f$ domain, and the relaxation time $\tau_{peak} = 1/2\pi f(\varepsilon''_{max})$, related to the maximal dielectric absorption, is related to τ_{HN} obtained from fitting by formula [15]:

$$\tau_{peak} = \tau_{HN}\left(\sin\left(\frac{\pi(1-a)}{2+2b}\right)\right)^{-\frac{1}{1-a}}\left(\sin\left(\frac{\pi(1-a)b}{2+2b}\right)\right)^{\frac{1}{1-a}} \quad (4)$$

For $b = 1$, $\tau_{peak} = \tau_{HN}$. Most of the relaxation processes observed for 5HF6 and 6HF6 are described by the Cole-Cole model (Figs. 5, 6). The only process with a significant asymmetry is the α-process in both homologues and the fragility index can be derived either from τ_{HN} or τ_{peak}. When one uses the Havriliak-Negami formula, it is more convenient to use τ_{HN}, however, in some complicated BDS spectra it can be easier to determine τ_{peak}. Moreover, the τ_{peak} value always corresponds to the local maximum in ε'', therefore it is not affected by the shape of the absorption peak,

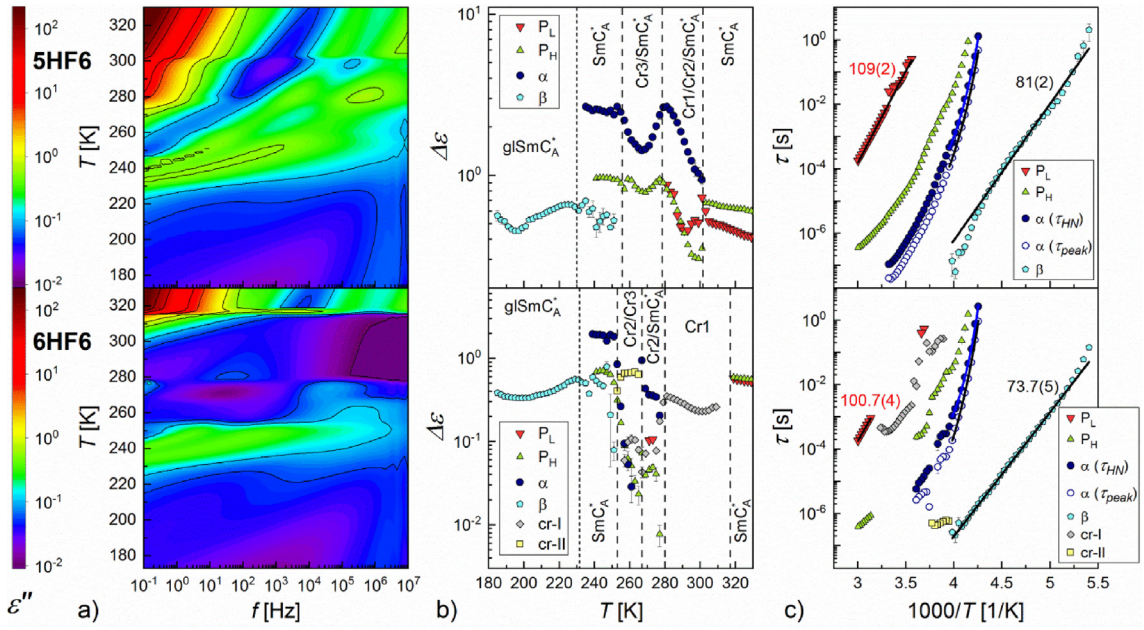

Fig. 4. BDS results for 5HF6 (upper panels) and 6HF6 (bottom panels) obtained upon heating after fast cooling: absorption part of dielectric spectra (a), dielectric strength vs temperature (b) and Arrhenius plots of the relaxation time (c). The isolines in (a) are drawn for ε'' = 0.01, 0.05, 0.1, 0.5, 1, 5, 10, 50, 100.

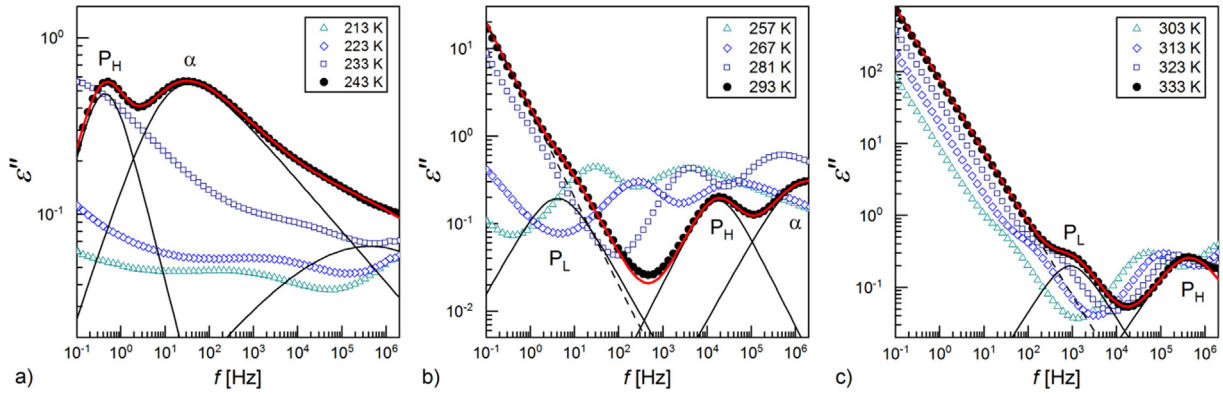

Fig. 5. Dielectric absorption of 5HF6 (points) and fitting results of Equation (3) (lines).

while τ_{HN} is. In this study, we are going to obtain m_f from both these characteristic times of the α-process and check to which extent it affects the final result.

5HF6 and 6HF6 cooled down to 173 K after previous heating to isotropic liquid are in the vitrified SmC_A^* phase. In the 173–230 K range, the β-process is observed, which has a small dielectric increment of 0.4–0.5 (Fig. 4b) and a wide, symmetric shape of the absorption peak. The relaxation time of the β-process decreases with increasing temperature in the Arrhenius manner and the activation energy is equal to 81(2) kJ/mol and 73.7(5) kJ/mol for 5HF6 and 6HF6, respectively (Fig. 4c). Similar activation energy values of the β-process were obtained for the 5HH6 compound [32] and also for the W-1000 and W-356 mixtures containing 5HF6 as one of the main components [34]. According to density functional theory (DFT) calculations [32,34] (Table 1), one can assume that the β process is not a genuine Johari-Goldstein process for the mX_1X_26 compounds and instead it is connected to correlated intra-molecular rotations of the benzene ring and biphenyl, each of them with the conformational energy barrier of 35 kJ/mol (results for 5HF6) [34].

Above ca. 230 K, the α-process appears in the investigated frequency range (Fig. 5a, 6a). Detailed analysis of the α-process was done only for the BDS spectra collected below the temperature of the beginning of cold crystallization: in the 235–253 K range for 5HF6 and 235–251 K for 6HF6. Fitting of the VFT formula to the relaxation time of the α-process gives parameters presented in Table 2. As it is shown in Fig. 4c, the relaxation time of the α process obtained as τ_{HN} is longer than τ_{peak} at the maximum of the dielectric absorption calculated using Equation (4). It leads to different fitting parameters of the VFT equation, especially B and τ_∞. However, the T_V and T_g temperatures are not significantly affected by the choice of the relaxation time. The glass transition temperature of ca. 230 K agrees with the glass softening temperature determined by differential scanning calorimetry [10]. The differences in m_f obtained from τ_{HN} and τ_{peak} are at the level of 4 % for 5HF6 and 13 % for 6HF6. The fragility calculated from τ_{HN} is significantly smaller for 5HF6 than for 6HF6, which implies that 6HF6 should crystallize easier [20]. It agrees with the DSC results presented in Ref. 10, as 6HF6 exhibited cold crystallization during heating with 3–20 K/min rates while 5HF6 remained in the supercooled SmC_A^* phase in the same conditions. On the other hand, the m_f values obtained from τ_{peak} are equal within uncertainties for both homologues, therefore the further analysis of τ_α and the crys-

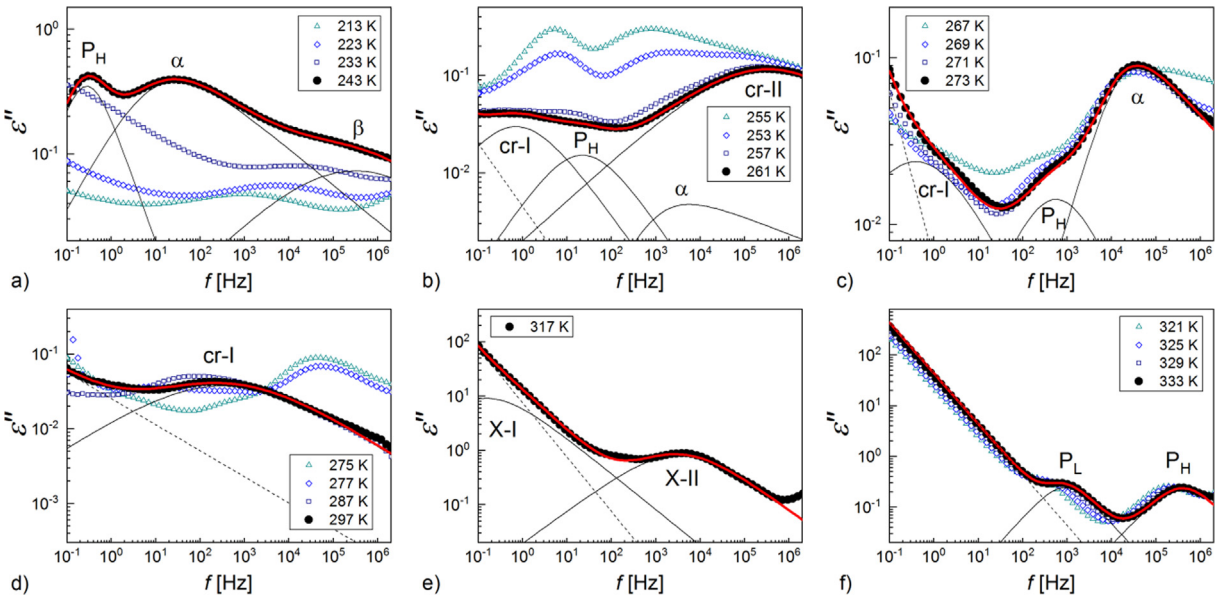

Fig. 6. Dielectric absorption of 6HF6 (points) and fitting results of Equation (3) (lines).

Table 1
Experimental activation energy E_β of the β-process compared with summed energy barriers for rotation of the benzene ring ΔE_{Ph} and rotation of biphenyl ΔE_{Ph-Ph} obtained from DFT calculations for the mX_1X_26 compounds. The W-1000 mixture contains 5HF6 and 7FH6 in the weight proportions of 0.53: 0.47 [34].

	E_β[kJ/mol]	ΔE_{Ph}[kJ/mol]	ΔE_{Ph-Ph}[kJ/mol]	$\Delta E_{Ph} + \Delta E_{Ph-Ph}$[kJ/mol]
5HF6	81(2)	35 [34]	35 [34]	70 [34]
6HF6	73.7(5)	–	–	–
5HH6	74.9(7) [32]	46.3 [32]	35 [32]	81.5
7FH6	–	40 [34]	35 [34]	75
W-1000	79.1(8) [34]	–	–	–

Table 2
Fitting parameters of the VFT formula to the relaxation time of the α-process and the glass transition temperature T_g and fragility index m_f derived from them.

compound	τ_α	$\log_{10}(\tau_\infty/s)$	B[K]	T_V[K]	T_g[K]	m_f
5HF6	$\tau_{HN}(T)$	−8.9(3)	583(33)	206.7(6)	230.1(2)	107.1(1.0)
	$\tau_{peak}(T)$	−10.1(1)	701(13)	204.0(2)	229.1(1)	111.0(4)
6HF6	$\tau_{HN}(T)$	−7.3(4)	359(36)	215.0(7)	231.7(4)	129.3(2.7)
	$\tau_{peak}(T)$	−11.2(4)	817(56)	203.1(8)	230.1(3)	112.1(1.0)

tallization time is necessary. Regardless of the definition of τ_α, the fragility of 5HF6 and 6HF6 is>100, thus they are classified as rather fragile glassformers.

Using the shape parameters a and b in the Havriliak-Negami formula (Equation (3)), one can estimate the n' parameter of the KWW function $\varphi(t) = \exp(-(t/\tau_\alpha)^{1-n'})$ [18] from the formula [46]:

$$(n')^{1.23} = (1-a)b \tag{5}$$

which gives the average value of n' equal to 0.37(2) for 5HF6 and 0.35(4) for 6HF6. Recently, Rams-Baron et al. [47] have shown that increasing n' value is accompanied by the increasing correlation length of the short-range order. The previous XRD study [10] has shown that correlation length within the smectic layers is only slightly smaller in 6HF6 than in 5HF6 (difference smaller than 1 Å in a wide temperature range), which agrees with similar n' values. After calculation of n', it is possible to check whether the Equation (2) is fulfilled for the studied compounds. The E_a/RT_g value equals 42.4 for 5HF6 and 41.6 for 6HF6, while the right-hand side equals 45.5–48.6 for 5HF6 and 43.1–47.8 for 6HF6, thus it is larger than the left-hand side of Equation (2), which indicates again that the β-process in this case is more probably a pseudo-JG process [36]. Relaxation processes observed in the SmC_A^* phase at higher temperatures are in-phase phason P_L with lower frequency and anti-phase phason P_H with higher frequency (Fig. 5b,c and 6c). These relaxation processes, as well as the processes in the SmC* and SmA* phases, were investigated in details and identified in [10]. The last process which requires interpretation is the α-process. As it was shown in [20], the relaxation process arising from the reorientations around the short molecular axes in the SmC_A^* phase overlaps with the P_L process, therefore is has much lower frequency than the α-process. It implies that the α-process in the SmC_A^* phase is the more likely related to reorientations around the long molecular axes. The origin of the α-process in the SmC_A^* phase was discussed also in our earlier paper [34].

The cold crystallization of 5HF6 begins above 253 K, which is visible as the decrease of Δε of the α-process (Fig. 4b). The Δε values of both processes reach a minimum at 267 K and at further heating up to 279 K they increase to values observed before cold crystallization. Such results are interpreted as partial cold crystallization to the Cr3 phase, followed by melting of Cr3 to the metastable SmC_A^* phase, as observed also in XRD results. Above

281 K, dielectric increment of the α-process decreases again with increasing temperature, which indicates the beginning of the SmC_A^* → Cr2 transition. Similar evolution of $\Delta\varepsilon$ with temperature is observed for the P_H process. The Cr2 → Cr1 transition, occurring around 290 K according to the XRD results, is not visible in the BDS spectra. The decrease of $\Delta\varepsilon$ values is observed up to 300 K, above this temperature Cr1 melts and the sample is in the stable SmC_A^* phase. During melting, the dielectric increment of the P_H process increases while the α-process is not observed anymore as it shifts above the upper frequency range. The only relaxation processes appearing in the dielectric spectra of 5HF6 are these characteristic of the SmC_A^* phase, no additional processes originating from the crystal phases are visible.

For 6HF6, interpretation of the BDS spectra during cold crystallization is more complicated, as there are two processes present in the crystal phases. The beginning of cold crystallization is visible above 251 K, where $\Delta\varepsilon$ values of the α- and P_H processes decrease with increasing temperature (Fig. 4b) and at the same time two new processes denoted as cr-I and cr-II appear (Fig. 6b). Above 267 K, the reappearance of the α- and P_H processes is observed, although their intensity does not reach the values obtained before cold crystallization, which suggest only a partial melting. According to the XRD results, the cold crystallization of 6HF6 results in co-existing Cr3 and Cr2 phases, with the Cr3 phase melting at ca. 268 K. Above 277 K, the α- and P_H processes disappear and the dielectric increment of the cr-I process increases, which is interpreted as the further development of the Cr2 phase. The Cr2 → Cr1 transition may be related to a slight decrease of the $\Delta\varepsilon$ of the cr-I process at 290 K. The relaxation time of the high-frequency cr-II process is weakly dependent on temperature, while for the low-frequency cr-I process, the relaxation time decreases with increasing temperature (Fig. 4c). The relaxation processes observed in the crystal phases of similar compounds were interpreted, based on DFT calculations, as intra-molecular rotations (e.g. rotation of the benzene ring in the molecular core or bending of the terminal chains) [32,33] and probably the same situation is for 6HF6. The assignment to the particular conformational changes cannot be done as the $\tau(T)$ dependences of the cr-I and cr-II processes are too scattered and deviate too much from the Arrhenius dependence to determine their activation energies.

During melting of the Cr1 phase at 317 K (Fig. 6e), two relaxation processes denoted as X-I and X-II are visible with relaxation times $9.1\cdot10^{-4}$ s and $8.7\cdot10^{-7}$ s, respectively. Both processes disappear after the Cr1 → SmC_A^* transition is completed. The X-I process resembles the low-frequency processes observed previously for pure mX_1X_26 compounds and their mixtures [32,34], related probably to the inhomogeneities in the sample [48], in this case at the crystal/smectic interface. The X-II process appears in the similar frequency region as the Goldstone mode in the ferroelectric SmC^* phase of 5HF6 and 6HF6 in higher temperatures [10]. We suppose that during melting of the crystal phase, where the interactions at the crystal/smectic interface contribute significantly to the molecular ordering, some fraction of the sample might exhibit a synclinic order of the molecular tilt in the neighbor smectic layers (typical for the SmC^* phase), which would enable the appearance of the Goldstone mode. After the thermodynamic equilibrium is set, the whole sample exhibits the anticlinic order and only the P_L and P_H processes characteristic of the SmC_A^* phase are observed (Fig. 6f).

3.2. Isothermal cold crystallization

3.2.1. Kinetics of crystallization

Crystallization degree $X(t)$ is a fraction of a sample which is in a crystal phase at time t. The $X(t)$ dependence can be calculated from the BDS spectra (Fig. 7a,b and Fig. S2 in SM) as [49]:

$$X(t) = 1 - \frac{\varepsilon'(t) - \varepsilon'_{end}}{\varepsilon'_{start} - \varepsilon'_{end}} \quad (6)$$

where $\varepsilon'(t)$ is a dielectric dispersion at time t at a selected frequency and ε'_{start}, ε'_{end} is a dielectric dispersion at the same frequency in the beginning and after crystallization, respectively. For 5HF6 and 6HF6, the $\varepsilon'(t)$ values at f = 0.1 Hz were selected. Next, the Avrami model [38–40] was used to describe the experimental $X(t)$ dependence:

$$X(t) = 1 - \exp\left(-\left(\frac{t - t_0}{\tau_{cr}}\right)^n\right) \quad (7)$$

where n is the Avrami exponent and t_0, τ_{cr} is the initialization time and characteristic time of crystallization, respectively. To analyze the $X(t)$ values from the BDS results (Fig. 7c), the Avrami formula was used in the form:

$$\ln(-\ln(1 - X)) = n\ln(t - t_0) - n\ln\tau_{cr} \quad (8)$$

which enables determination of n from a slope and τ_{cr} from an intercept of the line fitted to $\ln(-\ln(1-X))$ vs $\ln(t - t_0)$ plot (Table 3).

For 6HF6, the linear dependence in the Avrami plot for X between 0.1 and 0.9 was obtained for all considered T_{cr} with assumption of t_0 = 0. For 5HF6, a method presented by Avramov et al. (2005) [40] was used to determine the initialization time. In this method, t_0 is obtained as the initialization time for which the derivative $dX(t - t_0)/d\ln(t - t_0)$ has a peak value when $X = 1 - 1/e \approx 0.632$ [40]. The representative Avramov plot for T_{cr} = 257 K with the correct t_0 is presented in Fig. 7d, while Fig. 7e shows the crystallization degree at the peak value of $dX(t - t_0)/d\ln(t - t_0)$ for various choices of t_0. The correct t_0 can be determined from the parameters of the fitted line. The respective plots for other T_{cr} are shown in Fig. S3 in SM.

Next, the τ_{cr} and n values were obtained from the linear fits to the Avrami plots (Fig. 7f). For 5HF6, the Avrami plots deviate from the linear dependence in the beginning of crystallization, which indicates that the mechanism of crystallization changes during the development of a crystal phase. The Avrami exponent n = 2.6–2.9 for 6HF6 is larger than $n \approx 1.2$ for 5HF6 and does not depend significantly on T_{cr}. For the three-, two- and one-dimensional growth of crystallites, the Avrami exponent is expected to be 3–4, 2–3 and 1–2, respectively. In each case, the upper value refers to the situation with the constant nucleation rate and the lowest value - to the constant number of nuclei [40]. During cold crystallization, it can be assumed that a considerable fraction of nuclei is already formed below T_{cr}, therefore their number at T_{cr} can be treated as approximately constant or increasing very slowly during crystallization [50]. It means that for 6HF6, the obtained n values can be interpreted as growth of anisotropic crystallites (faster growth in two dimensions due to the flattened shape of a sample), while for 5HF6, the n value close to 1 implies 1-dimensional growth of needle-like crystallites. 6HF6 crystallizes faster than 5HF6 in the investigated T_{cr} range. As it is seen in Table 2, τ_{cr} of 6HF6 (0.8–2.5 h) is much shorter than t_0 (1.7–2.7 h) and τ_{cr} (2.4–4.3 h) of 5HF6 in the same T_{cr}.

3.2.2. Evolution of BDS spectra

Collection of the BDS spectra during isothermal cold crystallization was carried out until they were not changing anymore with time. However, even in the last registered spectra some relaxation processes are visible (Fig. 8 and Fig. S4, S5 in SM). For 5HF6 (Fig. 8, upper panel), the dielectric strength of the α-process decreases during cold crystallization but does not reach zero, therefore there is still a remaining fraction of the SmC_A^* phase even after the crystallization process slows down after several hours (Fig. 7c). The τ_{HN}

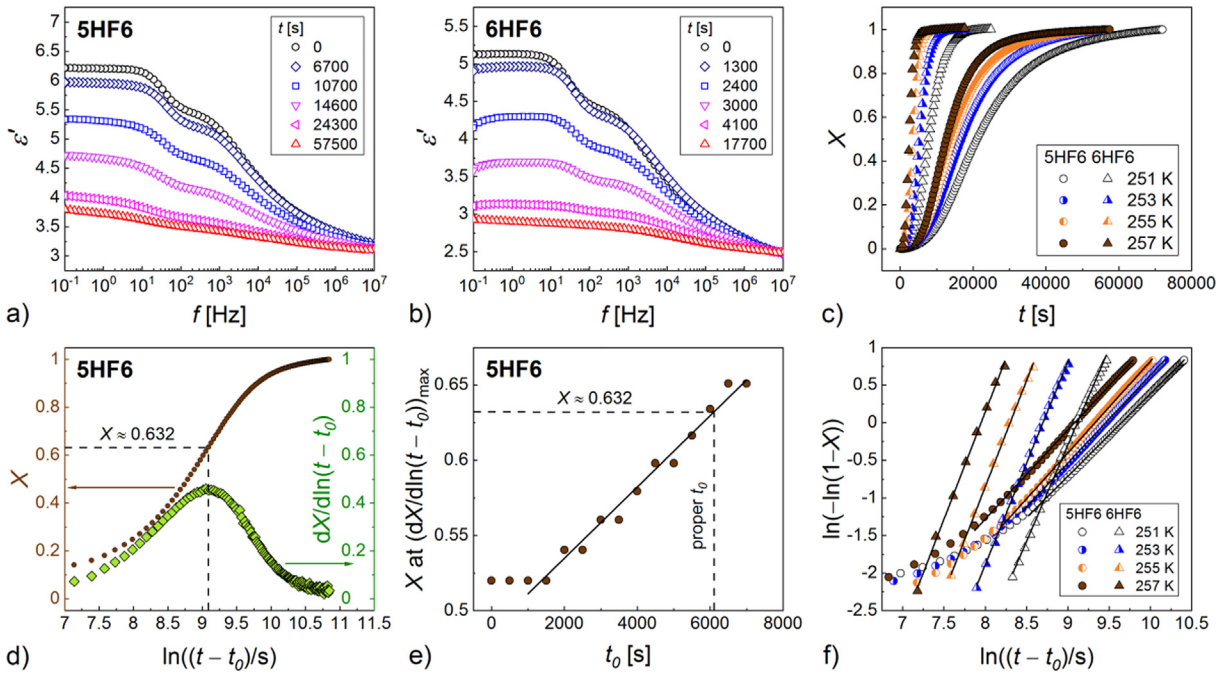

Fig. 7. Isothermal cold crystallization of 5HF6 and 6HF6 investigated by BDS: dielectric dispersion of 5HF6 (a) and 6HF6 (b) vs time during cold crystallization in 257 K; crystallization degree X vs time (c); Avrami-Avramov plot (d) and crystallization degree at maximum $dX/d\ln(t-t_0)$ for various choices of the initialization time t_0 (e) for the cold crystallization of 5HF6 in 257 K; and Avrami plots for both compounds (f).

Table 3
Parameters of the Avrami model describing the isothermal cold crystallization of mHF6 (m = 5, 6).

compound	T_{cr}[K]	t_0[s]	τ_{cr}[s]	n
5HF6	257	6110(430)	8810(430)	1.18(1)
	255	6000(410)	11270(410)	1.22(1)
	253	7350(380)	12810(380)	1.17(1)
	251	9860(400)	15520(400)	1.10(1)
6HF6	257	0	2835(17)	2.85(5)
	255	0	4027(14)	2.83(3)
	253	0	5993(18)	2.70(3)
	251	0	9093(28)	2.56(3)

values of the α-process increase with an increasing crystallization degree but the τ_{peak} values decrease for $X > 0.85$, which is caused by the increasing asymmetry of the absorption peak. For $X > 0.5$–0.8, depending on T_{cr}, a new process appears on the high-frequency side of the α-process. This new process is denoted as cr-process and originates from the crystal phase. It was not observed during non-isothermal cold crystallization (Fig. 4) probably because the fraction of a crystal phase in the sample was too small. The dielectric increment of the P_H process increases slightly during the initial stages of crystallization (maximal $\Delta\varepsilon$ for $X = 0.1$–0.2, Fig. 8b, upper panel). Afterwards, the P_H process decreases in strength but does not disappear completely. The relaxation time of the P_H process

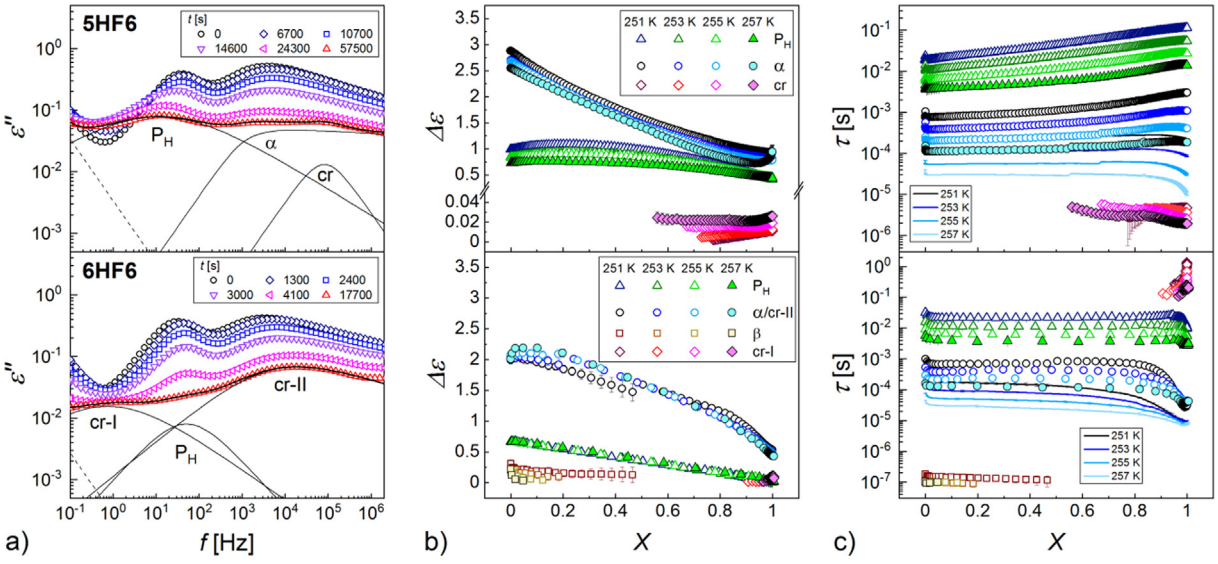

Fig. 8. Evolution of the dielectric absorption at 257 K (a), and dielectric increment (b) and relaxation time (c) vs crystallization degree during the cold crystallization of 5HF6 (upper panels) and 6HF6 (bottom panels). The legends in (b) apply also to the respective panels from (c). For the α-process, τ_{HN} and τ_{peak} values in (c) are denoted by points and lines, respectively.

increases during the whole crystallization process (Fig. 8c, upper panel). It might be related to the spatial confinement caused by low-dimensional crystallites because it is not observed for 6HF6, where the Avrami parameter is larger.

Different evolution of the BDS spectra occurs for 6HF6 (Fig. 8, bottom panel). Although the P_H process can be still noticed in the last registered spectra for each T_{cr}, its $\Delta\varepsilon$ decreases by more than two orders of magnitude during crystallization, therefore the fraction of the remaining SmC_A^* phase is negligible. The relaxation time of the P_H process is constant during the almost whole crystallization, except the last stage ($X > 0.95$) when τ slightly decreases. The diminishing α-process is strongly overlapped with the arising cr-II process, therefore they were fitted as a single process, which led to the inflection in the $\Delta\varepsilon(X)$ and $\tau(X)$ dependences for X = 0.8–0.85. The cr-II process can be included in fitting only for $X > 0.9$, as for the earlier stages of crystallization it is hidden in the conductivity contribution.

3.2.3. Coupling between τ_α and τ_{cr}

The characteristic time τ_{cr} of the isothermal cold crystallization of 5HF6 and 6HF6 changes with the crystallization temperature T_{cr} and the dependence is Arrhenius-like (Fig. 9a). The activation energy determined for 6HF6 is equal to 106(3) kJ/mol. For 5HF6, despite much larger τ_{cr} values, the activation energy is about two times smaller and equal to 48(4) kJ/mol. As it was shown in Refs. 41 and 42, the crystallization rate/crystallization time is coupled with the relaxation time of the α-process: $\tau_{cr} = \tau_\alpha^\xi$, where ξ is the coupling coefficient. Such coupling is observed also for 5HF6 and 6HF6 (Fig. 9b). The slope of the $\ln\tau_{cr}$ vs $\ln\tau_\alpha$ plot does not depend whether one chooses the τ_{HN} or τ_{peak} values of the α-process. The coupling coefficient ξ equals 0.64 for 6HF6, while for 5HF6 it is much smaller and equals 0.26–0.27. The ξ coefficient usually increases with decreasing m_f; the empirical formula obtained in Ref. 41 based on numerous experimental data is $\xi \approx 1.1 - 0.005m_f$. Using Equation (8) and the m_f values of 5HF6 and 6HF6 from Table 1, one obtains $\xi \approx$ 0.45–0.56 (with uncertainty of 0.05 [41]), which, especially for 5HF6, differs from ξ determined from the slope of the $\ln\tau_{cr}$ vs $\ln\tau_\alpha$ plot (Table 4). It can arise from the fact that the empirical formula from Ref. 41 was based on data for isotropic glassformers, while 5HF6 and 6HF6 form the SmC_A^* glass, which is anisotropic and possesses partial positional ordering.

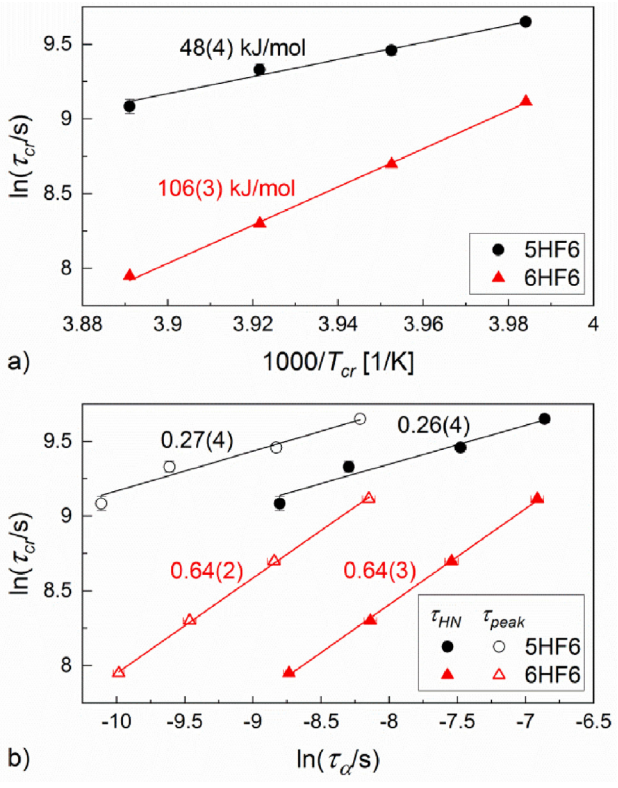

Fig. 9. Arrhenius plot of the characteristic time τ_{cr} of cold crystallization (a) and coupling between τ_{cr} and relaxation time τ_α of the α-process (b).

The obtained results show that the molecular mobility has a more significant influence on the kinetics of cold crystallization for 6HF6 than for 5HF6. Fast decrease of τ_{cr} with increasing T_{cr} together with the coupling coefficient ξ = 0.64 for 6HF6 imply that the diffusion rate has a decisive role in the crystallization rate, which is in agreement with an assumption of the constant number of nuclei [49,50]. For 5HF6, both the activation energy and coupling coefficient are smaller, indicating that the nucleation rate influences the crystallization kinetics more than for 6HF6, although the diffusion rate has still a more prominent role. Nucleation rate increases with the increasing thermodynamic driving force, which can be estimated as $\Delta G \approx \Delta S_m \Delta T$, where ΔS_m is the entropy of melting and $\Delta T = T_m - T_{cr}$ is the undercooling [41,42]. Taking into account the melting temperatures T_m and enthalpy of melting ΔH_m reported in Ref. [6] for the most stable crystal phases, we obtain ΔG = 5.1–5.8 kJ/mol and 6.3–7.0 kJ/mol for 5HF6 and 6HF6, respectively, in the 251–257 K range, and 8.3 kJ/mol and 9.3 kJ/mol at $T_g \approx$ 230 K. Although cold crystallization in 251–257 K does not result in the most stable crystal phases, their nuclei can be already formed and serving as additional centers of heterogeneous nucleation for less stable crystal phases. In that case, smaller ΔG for 5HF6 can result in the smaller number of nuclei during cold crystallization.

At this point we would like to mention the previous results [12,51] for the 7HF6 and 7FF6 compounds from the mX_1X_26 family. 7HF6 is a glassformer while 7FF6 crystallizes on fast cooling of 20 K/min. Comparison of their BDS spectra revealed that the P_H process in the SmC_A^* phase (α-process was not observed for 7FF6) was characterized by the smaller relaxation time in 7HF6 than in 7FF6, which we suspected to be correlated with easier crystallization of 7FF6. Fig. 10 shows the ratios of the relaxation times of p_H and α-processes in 5HF6 and 6HF6. The relaxation time of the P_H process is smaller for 5HF6 than for 6HF6 and their ratio decreases with decreasing temperature. Faster P_H process in 5HF6 is correlated with larger crystallization time than for 6HF6, which is in agreement with the previous observations for 7HF6 and 7FF6. At present it is not certain if this is a causal relation or rather a correlation with a common origin, namely the intermolecular interactions within the SmC_A phase. However, our supposition is that the faster P_H process, which is a collective fluctuation of the order parameter, decreases the probability of the formation of stable nuclei of crystallization. The relaxation time of the α-process, both τ_{HN} and τ_{peak}, is also smaller for 5HF6 at 245 K and below, while above 245 K the results are scattered around 1. Faster α-process in 5HF6 would be expected to increase the crystal growth rate. However, from the results in Fig. 9b one can deduce that the coupling between τ_α and τ_{cr} is much weaker than for

Table 4
Coupling coefficient ξ between τ_{cr} of the cold crystallization and relaxation time τ_α of the α-process.

compound	τ_α	$\ln\tau_{cr}$ vs $\ln\tau_\alpha$ slope	$1.1 - 0.005m_f$
5HF6	$\tau_{HN}(T)$	0.26(4)	0.56(5)
	$\tau_{peak}(T)$	0.27(4)	0.54(5)
6HF6	$\tau_{HN}(T)$	0.64(3)	0.45(5)
	$\tau_{peak}(T)$	0.64(2)	0.54(5)

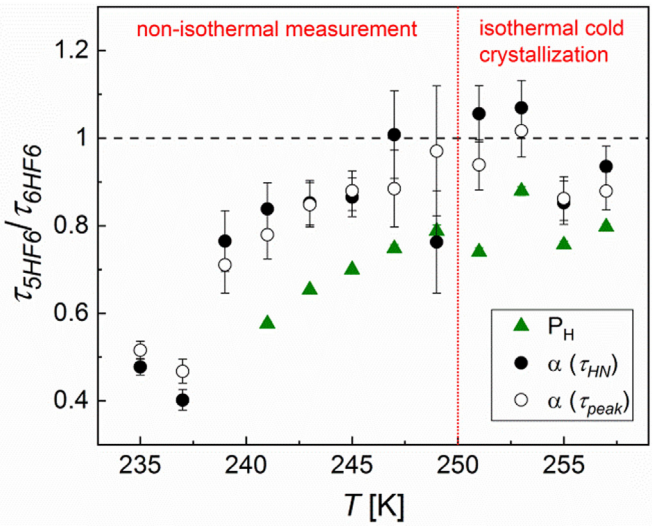

Fig. 10. Ratios of the relaxation times of 5HF6 and 6HF6 in the supercooled SmC_A^* phase.

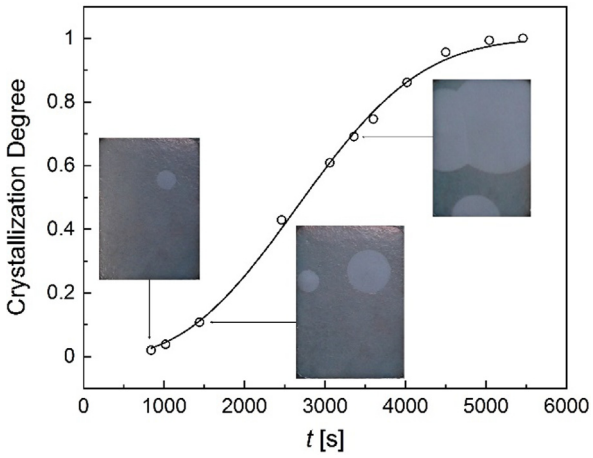

Fig. 11. Crystallization degree vs time for the melt crystallization of 6HF6 together with selected photos taken during the process.

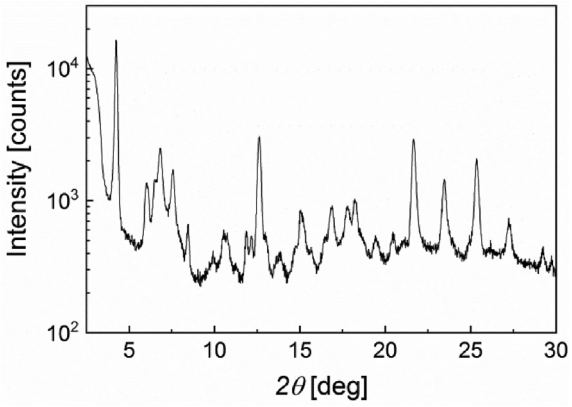

Fig. 12. XRD pattern of 6HF6 after melt crystallization in the room temperature.

6HF6. Our interpretation is that a lower nucleation rate in 5HF6, caused either by the smaller thermodynamic driving force and/or by the faster P_H process, leads to slower crystallization than for 6HF6, despite the slightly faster α-process in 5HF6.

The results for 5HF6 and 6HF6 presented here together with the previous results for the mHF6 series show that the length of the -C_mH_{2m}- chain influences strongly the ability of a given homologue to form the SmC_A^* glass. 5HF6 and 6HF6 vitrify in the SmC_A^* phase at low cooling rate of 3 K/min [10], as does the longer 7HF6 homologue [12]. Among the homologues with the shorter -C_mH_{2m}-chain, 2HF6 and 4HF6 show the crystallization during cooling at 3–20 K/min (although for 4HF6, some fraction of the SmC_A^* phase vitrifies during cooling at 15 and 20 K/min) [10]. 3HF6 is probably a glass-former, as only a small fraction of the sample crystallizes during slow cooling at 2.5 K/min down to ca. 263 K and a large exothermic anomaly related to the cold crystallization is observed on heating in the DSC scans [52]. The conclusion is that the tendency to form the SmC_A^* glass by mHF6 homologues increases with the increasing length of the -C_mH_{2m}- chain and, additionally, it is higher for the odd homologues. The latter observation corresponds to the fact that odd mHF6 homologues have a much wider stability range of the SmC_A^* phase than even homologues [6].

3.3. Melt crystallization of 6HF6

The previous XRD results for 6HF6 [10] show that although this compound exhibits the vitrified SmC_A^* phase on cooling, a small fraction of the sample crystallizes when the cooling occurs very slowly. It means that 6HF6 can undergo a melt crystallization. In this study we show that 6HF6 crystallizes in isothermal conditions after cooling to the room temperature. Fig. 11 shows representative photos taken during crystallization and the crystallization degree, determined as the ratio of the sample area containing a crystal phase and the total area of the sample [27]. The melt crystallization was investigated for a substance in the sample holder used in the XRD measurements, which enabled a visual observation. Analysis by the Avrami model, performed by fitting of the Avrami formula in the form given by Equation (7), leads to values n = 2.7(1) and τ_{cr} = 3129(25) s. The initialization time was equal to zero within the uncertainties of the fitting, therefore it was set to zero before the final calculations. Optical observation of the whole sample during crystallization allows to say undoubtedly that this is the 2-dimensional growth of crystals with a discoidal shape. Only three crystallites are formed during crystallization, therefore the nucleation rate is very low. It is in agreement with the corresponding n value and it supports also the previous interpretation of the Avrami exponent for isothermal cold crystallization. The XRD pattern collected after the isothermal crystallization of 6HF6 in the room temperature indicates the Cr1 phase (Fig. 12).

4. Summary and conclusions

Two mHF6 homologues (m = 5, 6), with different length of the -C_mH_{2m}- chain, were investigated with the BDS and XRD methods. Both methods indicate the presence of three crystal phases for each compound upon slow heating from the vitrified SmC_A^* phase. The BDS method was applied also to compare the kinetics of isothermal cold crystallization in 251–257 K. The characteristic crystallization time of 6HF6 is much shorter than that of 5HF6, in the studied temperature range. For both homologues the diffusion rate has more impact on the crystallization kinetics than the nucleation rate, however, for 6HF6 this impact is more significant than for 5HF6. Additionally, the coupling between the characteristic crystallization time and the relaxation time of the α-process in the SmC_A^* phase is stronger in 6HF6 than in 5HF6. Both investigated homologues have a high fragility index > 100. The fragilities of 5HF6 and 6HF6 are similar, therefore differences in their fragility cannot serve as explanation of differences in their crystallization rates. It

should be kept in mind that mHF6 compounds are not usual glass-formers, where the vitrified phase is isotropic liquid. Instead, they exhibit the glass of the liquid crystalline SmC_A^* phase, which possesses a quasi-long-range order in one dimension. This is why our proposition is to pay attention to another relaxation process characteristic of the SmC_A^* phase, which is the anti-phase phason P_H. Our BDS results suggest that the shorter relaxation time of the P_H process is correlated with slower crystallization. We observed this for the 5HF6, 6HF6 pair investigated in this paper, and also for the 7HF6, 7FF6 pair from the previous study. Future investigations for other mX_1X_26 compounds will reveal whether this observation is indeed a rule.

CRediT authorship contribution statement

Aleksandra Deptuch: Conceptualization, Investigation, Formal analysis, Visualization, Writing – original draft. **Małgorzata Jasiurkowska-Delaporte:** Investigation, Writing – review & editing. **Magdalena Urbańska:** Resources, Writing - review & editing. **Stanisław Baran:** Investigation, Writing – review & editing.

Data availability

Data will be made available on request.

Declaration of Competing Interest

The authors declare that they have no known competing financial interests or personal relationships that could have appeared to influence the work reported in this paper.

Acknowledgement

Empyrean 2 (PANalytical) diffractometer with Cryostream 700 Plus (Oxford Cryosystems) temperature attachment were purchased thanks to European Regional Development Fund Operational Program Infrastructure and Environment (contract no. POIS.13.01.00-00-062/08).

Appendix A. Supplementary material

Supplementary data to this article can be found online at https://doi.org/10.1016/j.molliq.2022.120612.

References

[1] K. D'havé, P. Rudquist, S.T. Lagerwall, H. Pauwels, W. Drzewinski, R. Dabrowski, Solution of the dark state problem in antiferroelectric liquid crystal displays, Appl. Phys. Lett. 76 (24) (2000) 3528–3530.
[2] K. D'havé, A. Dahlgren, P. Rudquist, J.P.F. Lagerwall, G. Andersson, M. Matuszczyk, S.T. Lagerwall, R. Dabrowski, W. Drzewinski, Antiferroelectric liquid crystals with 45° tilt - a new class of promising electro-optic materials, Ferroelectrics 244 (1) (2000) 115–128.
[3] S.T. Lagerwall, A. Dahlgren, P. Jägemalm, P. Rudquist, K. D'havé, H. Pauwels, R. Dabrowski, W. Drzewinski, Unique Electro-Optical Properties of Liquid Crystals Designed for Molecular Optics, Adv. Funct. Mater. 11 (2) (2001) 87–94.
[4] R. Dąbrowski, J. Gąsowska, J. Otón, W. Piecek, J. Przedmojski, M. Tykarska, High tilted antiferroelectric liquid crystalline materials, Displays 25 (2004) 9–19, https://doi.org/10.1016/j.displa.2004.04.002.
[5] M. Żurowska, R. Dąbrowski, J. Dziaduszek, K. Czupryński, K. Skrzypek, M. Filipowicz, Synthesis and Mesomorphic Properties of Chiral Esters Comprising Partially Fluorinated Alkoxyalkoxy Terminal Chains and a 1-methylheptyl Chiral Moiety Mol. Cryst. Liq. Cryst. 495 (2008) 145/[497]-157/[509], 10.1080/15421400802432428.
[6] M. Żurowska, R. Dąbrowski, J. Dziaduszek, K. Garbat, M. Filipowicz, M. Tykarska, W. Rejmer, K. Czupryński, A. Spadło, N. Bennis, J.M. Otón, Influence of alkoxy chain length and fluorosubstitution on mesogenic and spectral properties of high tilted antiferroelectric esters, J. Mater. Chem. 21 (2011) 2144–2153, https://doi.org/10.1039/C0JM02015J.
[7] K. Milewska, W. Drzewiński, M. Czerwiński, R. Dąbrowski, Design, synthesis and mesomorphic properties of chiral benzoates and fluorobenzoates with direct SmC_A^*-Iso phase transition, Liq. Cryst. 42 (2015) 1601–1611, https://doi.org/10.1080/02678292.2015.1078916.
[8] J. Fitas, A. Dłubacz, P. Fryń, M. Marzec, T. Jaworska-Gołąb, A. Deptuch, K. Kurp, M. Tykarska, M. Żurowska, New ferroelectric and antiferroelectric liquid crystals studied by complementary methods, Liq. Cryst. 44 (2017) 566–576, https://doi.org/10.1080/02678292.2016.1225841.
[9] M. Żurowska, M. Filipowicz, M. Czerwiński, M. Szala, Synthesis and properties of ferro- and antiferroelectric esters with a chiral centre based on (S)-(+)-3-octanol, Liq. Cryst. 46 (2019) 299–308, https://doi.org/10.1080/02678292.2018.1499147.
[10] A. Deptuch, M. Marzec, T. Jaworska-Gołąb, M. Dziurka, J. Hooper, M. Srebro-Hooper, P. Fryń, J. Fitas, M. Urbańska, M. Tykarska, Influence of carbon chain length on physical properties of 3FmHPhF homologues, Liq. Cryst. 46 (2019) 2201–2212, https://doi.org/10.1080/02678292.2019.1614685.
[11] P. Morawiak, M. Żurowska, W. Piecek, A long-pitch orthoconic antiferroelectric mixture modified by isomeric and racemic homostructural dopants, Liq. Cryst. 45 (2018) 1451–1459, https://doi.org/10.1080/02678292.2018.1446555.
[12] A. Deptuch, T. Jaworska-Gołąb, M. Marzec, D. Pociecha, J. Fitas, M. Żurowska, M. Tykarska, J. Hooper, Mesomorphic phase transitions of 3F7HPhF studied by complementary methods, Phase Trans. 91 (2018) 186–198, https://doi.org/10.1080/01411594.2017.1393814.
[13] A. Deptuch, T. Jaworska-Gołąb, M. Marzec, M. Urbańska, M. Tykarska, Magdalena Urbańska, Marzena Tykarska, Cold crystallization from chiral smectic phase, Phase Trans. 92 (2) (2019) 126–134.
[14] W. Haase, S. Wróbel (Eds.), Relaxation phenomena. Liquid crystals, magnetic systems, polymers, high-Tc superconductors, metallic glasses, Springer-Verlag, Berlin Heidelberg 2003, 10.1007/978-3-662-09747-2.
[15] F. Kremer, A. Schönhals (Eds.), Broadband Dielectric Spectroscopy, Springer-Verlag, Berlin Heidelberg 2003, 10.1007/978-3-642-56120-7.
[16] M.D. Ediger, C.A. Angell, S.D. Nagel, Supercooled Liquids and Glasses, J. Phys. Chem. 100 (1996) 13200–13212, https://doi.org/10.1021/jp953538d.
[17] G.P. Johari, J.W. Goodby, Dielectric relaxations in a supercooled liquid and glassy smectic phase, J. Chem. Phys. 77 (1982) 5165–5172, https://doi.org/10.1063/1.443693.
[18] S. Kripotou, D. Georgopoulos, A. Kyritsis, P. Pissis, Phase Transitions and Molecular Mobility in 5CB and CE8 Studied by Dielectric Techniques, Mol. Cryst. Liq. Cryst. 623 (2015) 407–423, https://doi.org/10.1080/15421406.2015.1066551.
[19] C. Filipič, T. Carlsson, A. Levstik, B. Žekš, R. Blinc, F. Gouda, S.T. Lagerwall, K. Skarp, Dielectric properties near the smectic-C*–smectic-A phase transition of some ferroelectric liquid-crystalline systems with a very large spontaneous polarization, Phys. Rev. A 38 (1988) 5833–5839, https://doi.org/10.1103/PhysRevA.38.5833.
[20] M. Buivydas, F. Gouda, G. Andersson, S.T. Lagerwall, B. Stebler, J. Bomelburg, G. Heppke, B. Gestblom, Collective and non-collective excitations in antiferroelectric and ferrielectric liquid crystals studied by dielectric relaxation spectroscopy and electro-optic measurements, Liq. Cryst. 23 (1997) 723–739, https://doi.org/10.1080/026782997208000.
[21] Y.P. Panarin, O. Kalinovskaya, J.K. Vij, The investigation of the relaxation processes in antiferroelectric liquid crystals by broad band dielectric and electro-optic spectroscopy, Liq. Cryst. 25 (1997) 241–252, https://doi.org/10.1080/026782998206399.
[22] S. Havriliak, S. Negami, A complex plane analysis of α-dispersions in some polymer systems, J. Polym. Sci. C: Polymer Symposia 14 (1966) 99–117, https://doi.org/10.1002/polc.5070140111.
[23] G. William, D.C. Watts, Non-symmetrical dielectric relaxation behaviour arising from a simple empirical decay function, Trans. Faraday Soc. 66 (1970) 80–85, https://doi.org/10.1039/TF9706600080.
[24] R. Böhmer, K.L. Ngai, C.A. Angell, D.J. Plazek, Nonexponential relaxations in strong and fragile glass formers, J. Chem. Phys. 99 (1993) 4201–4209, https://doi.org/10.1063/1.466117.
[25] H. Tanaka, Relationship among glass-forming ability, fragility, and short-range bond ordering of liquids, J. Non-Cryst. Solids 351 (2005) 678–690, https://doi.org/10.1016/j.jnoncrysol.2005.01.070.
[26] M. Jasiurkowska-Delaporte, M. Massalska-Arodź, Molecular dynamics of 4-propyl-4′-thiocyanatobiphenyl (3BT) in the strong glass-forming smectic E phase, J. Mol. Liq. 241 (2017) 355–358, https://doi.org/10.1016/j.molliq.2017.06.027.
[27] T. Rozwadowski, M. Massalska-Arodź, Ł. Kolek, K. Grzybowska, A. Bąk, K. Chłędowska, Kinetics of Cold Crystallization of 4-Cyano-3-fluorophenyl 4-Butylbenzoate (4CFPB) Glass Forming Liquid Crystal. I. Nonisothermal Process As Studied by Microscopic, Calorimetric, and Dielectric Methods, Crystal Growth & Design 15 (6) (2015) 2891–2900.
[28] M. Jasiurkowska-Delaporte, T. Rozwadowski, E. Dmochowska, E. Juszyńska-Gałązka, P. Kula, M. Massalska-Arodź, Interplay between Crystallization and Glass Transition in Nematic Liquid Crystal 2,7-Bis(4-pentylphenyl)-9,9-diethyl-9*H*-fluorene, J. Phys. Chem. B 122 (2018) 10627–10636, https://doi.org/10.1021/acs.jpcb.8b08138.
[29] M. Jasiurkowska-Delaporte, T. Rozwadowski, E. Juszyńska-Gałązka, J. Krawczyk, E. Dmochowska, P. Kula, M. Massalska-Arodź, Relaxation dynamics and crystallization study of glass-forming chiral-nematic liquid crystal S, S-2,7-bis(4-pentylphenyl)-9,9-dimethylbutyl 9H-fluorene (5P-Am*FLAm*-P5), Eur. Phys. J. E 42 (2019) 121, https://doi.org/10.1140/epje/i2019-11887-6.
[30] Ł. Kolek, M. Jasiurkowska-Delaporte, M. Massalska-Arodź, W. Szaj, T. Rozwadowski, Mesomorphic and dynamic properties of 3F5BFBiHex

antiferroelectric liquid crystal as reflected by polarized optical microscopy, differential scanning calorimetry and broadband dielectric spectroscopy, J. Mol. Liq. 320 (2020), https://doi.org/10.1016/j.molliq.2020.114338.
[31] A. Drzewicz, M. Jasiurkowska-Delaporte, E. Juszyńska-Gałązka, W. Zając, P. Kula, On the relaxation dynamics of a double glass-forming antiferroelectric liquid crystal, Phys. Chem. Chem. Phys. 23 (2021) 8673–8688, https://doi.org/10.1039/D0CP06203K.
[32] A. Deptuch, M. Jasiurkowska-Delaporte, W. Zając, E. Juszyńska-Gałązka, A. Drzewicz, M. Urbańska, Investigation of crystallization kinetics and its relationship with molecular dynamics for chiral fluorinated glassforming smectogen 3F5HPhH6, Phys. Chem. Chem. Phys. 23 (2021) 19795–19810, https://doi.org/10.1039/D1CP02297K.
[33] A. Drzewicz, M. Jasiurkowska-Delaporte, E. Juszyńska-Gałązka, A. Deptuch, M. Gałązka, W. Zając, W. Drzewiński, On relaxation and vibrational dynamics in the thermodynamic states of a chiral smectogenic glass-former, Phys. Chem. Chem. Phys. 24 (2022) 4595–4612, https://doi.org/10.1039/D1CP05048F.
[34] A. Deptuch, S. Lalik, M. Jasiurkowska-Delaporte, E. Juszyńska-Gałązka, A. Drzewicz, M. Urbańska, M. Marzec, Comparative study of electrooptic, dielectric, and structural properties of two glassforming antiferroelectric mixtures with a high tilt angle, Phys. Rev. E 105 (2022), https://doi.org/10.1103/PhysRevE.105.024705.
[35] G.P. Johari, M. Goldstein, Viscous Liquids and the Glass Transition. II. Secondary Relaxations in Glasses of Rigid Molecules, J. Chem. Phys. 53 (1970) 2372–2388, https://doi.org/10.1063/1.1674335.
[36] K.L. Ngai, M. Paluch, Classification of secondary relaxation in glass-formers based on dynamic properties, J. Chem. Phys. 120 (2004) 857–873, https://doi.org/10.1063/1.1630295.
[37] K.L. Ngai, S. Capaccioli, Relation between the activation energy of the Johari-Goldstein β relaxation and T_g of glass formers, Phys. Rev. E 69 (2004), https://doi.org/10.1103/PhysRevE.69.031501.
[38] M. Avrami, Kinetics of Phase Change. I General Theory, J. Chem. Phys. 7 (1939) 1103–1112, https://doi.org/10.1063/1.1750380.
[39] M. Avrami, Kinetics of Phase Change. II Transformation-Time Relations for Random Distribution of Nuclei, J. Chem. Phys. 8 (1940) 212–224, https://doi.org/10.1063/1.1750631.
[40] I. Avramov, K. Avramova, C. Rüssel, New method to analyze data on overall crystallization kinetics, Cryst. Growth Des. 285 (2005) 394–399, https://doi.org/10.1016/j.jcrysgro.2005.08.024.
[41] M.D. Ediger, P. Harrowell, L. Yu, Crystal growth kinetics exhibit a fragility-dependent decoupling from viscosity, J. Chem. Phys. 128 (2008), https://doi.org/10.1063/1.2815325.
[42] A. Sanz, K. Niss, Coupling between Molecular Mobility and Kinetics of Crystal Growth in a Hydrogen-Bonded Liquid, Cryst. Growth Des. 17 (2017) 4628–4636, https://doi.org/10.1021/acs.cgd.7b00484.
[43] T. Roisnel, J. Rodriguez-Carvajal, WinPLOTR: a Windows tool for powder diffraction patterns analysis, Materials Science Forum 378–381 (2000) 118–123, https://doi.org/10.4028/www.scientific.net/MSF.378-381.118.
[44] G. Vertogen, W. H. de Jeu, Thermotropic Liquid Crystals. Fundamentals, Springer-Verlag, Berlin Heidelberg 1988, 10.1007/978-3-642-83133-1.
[45] K.S. Cole, R.H. Cole, Dispersion and Absorption in Dielectrics I. Alternating Current Characteristics, J. Chem. Phys. 9 (1941) 341–351, https://doi.org/10.1063/1.1750906.
[46] F. Alvarez, A. Alegría, J. Colmenero, Relationship between the time-domain Kohlrausch-Williams-Watts and frequency-domain Havriliak-Negami relaxation functions, Phys. Rev. B 44 (1991) 7306–7312, https://doi.org/10.1103/PhysRevB.44.7306.
[47] M. Rams-Baron, A. Jędrzejowska, K. Jurkiewicz, M. Matussek, K.L. Ngai, M. Paluch, Broadband Dielectric Study of Sizable Molecular Glass Formers: Relationship Between Local Structure and Dynamics, J. Phys. Chem. Lett. 12 (2021) 245–249, https://doi.org/10.1021/acs.jpclett.0c03377.
[48] V. Novotná, M. Glogarová, A.M. Bubnov, H. Sverenyák, Thickness dependent low frequency relaxations in ferroelectric liquid crystals with different temperature dependence of the helix pitch, Liq. Cryst. 23 (1997) 511–518, https://doi.org/10.1080/026782997208091.
[49] M. Massalska-Arodź, G. Williams, I.K. Smith, C. Conolly, G.A. Aldridge, R. Dąbrowski, Molecular dynamics and crystallization behaviour of isopentyl cyanobiphenyl as studied by dielectric relaxation spectroscopy, J. Chem. Soc., Faraday Trans. 94 (1998) 387–394, https://doi.org/10.1039/A706225G.
[50] K. Kołodziejczyk, M. Paluch, K. Grzybowska, A. Grzybowski, Z. Wojnarowska, L. Hawelek, J.D. Zioło, Relaxation Dynamics and Crystallization Study of Sildenafil in the Liquid and Glassy States, Mol. Pharm. 10 (2013) 2270–2282, https://doi.org/10.1021/mp300479r.
[51] A. Deptuch, A. Drzewicz, M. Dziurka, N. Górska, J. Hooper, T. Jaworska-Gołąb, E. Juszyńska-Gałązka, M. Marzec, M. Piwowarczyk, M. Srebro-Hooper, M. Tykarska, M. Urbańska, Influence of fluorosubstitution on physical properties of the smectogenic chiral ester, Mater. Res. Bull. 150 (2022), https://doi.org/10.1016/j.materresbull.2022.111756.
[52] A. Mishra, R. Dąbrowski, R. Dhar, Dielectric characteristics of highly ionic antiferroelectric liquid crystalline material, J. Mol. Liq. 249 (2018) 106–109, https://doi.org/10.1016/j.molliq.2017.11.025.